

Structure of the ground and excited states in ${}^9_{\Lambda}\text{Be}$ nucleus

Yu. A. Lashko,* A. V. Nesterov,† and V. S. Vasilevsky‡
*Bogolyubov Institute for Theoretical Physics,
 14-b Metrolohichna str., 03143, Kiev, Ukraine*

We investigate properties of bound and resonance states in the ${}^9_{\Lambda}\text{Be}$ nucleus. To reveal the nature of these states, we use a three-cluster $2\alpha + \Lambda$ microscopic model. The model incorporates Gaussian and oscillator basis functions and reduces a three-cluster Schrödinger equation to a two-body like many-channel problem with the two-cluster subsystems (${}^5_{\Lambda}\text{He}$ and ${}^8\text{Be}$) being in a bound or a pseudo-bound state. Influence of the cluster polarization on the energy and widths of resonance states in ${}^9_{\Lambda}\text{Be}$ and on elastic and inelastic ${}^5_{\Lambda}\text{He} + \alpha$ scattering is analysed.

I. INTRODUCTION

We apply a microscopic three-cluster model to study the hypernucleus ${}^9_{\Lambda}\text{Be}$. This nucleus is considered as a three-cluster system $\alpha + \alpha + \Lambda$. Our aim is to examine both discrete and continuous spectrum states of ${}^9_{\Lambda}\text{Be}$. This research is performed within a microscopic three-cluster model referred as AMGOB (the Algebraic Model of scattering with the Gaussian and Oscillator Bases). This model was formulated in Ref. [1]. Recently we successfully applied AMGOB model for studying ${}^{10}\text{Be}$ nucleus [2]. AMGOB model reduces a three-cluster problem to a many-channel problem with two-body states in incoming and outgoing channels. By this reason, the model is particularly appealing for investigating different two-body decay channels of the compound hypernucleus.

The energy of $1/2^+$ ground state in ${}^9_{\Lambda}\text{Be}$ is -3.12 MeV with respect to its lowest binary decay threshold ${}^9_{\Lambda}\text{Be} \rightarrow {}^5_{\Lambda}\text{He} + \alpha$ and -6.63 MeV relative to its three-cluster $2\alpha + \Lambda$ threshold. Unlike ${}^9\text{Be}$, which is a Borromean nucleus, ${}^9_{\Lambda}\text{Be}$ has a bound two-body subsystem ${}^5_{\Lambda}\text{He}$. That is why it is important to take into account the possibility for the ${}^9_{\Lambda}\text{Be}$ hypernucleus to decay via ${}^9_{\Lambda}\text{Be} \rightarrow {}^5_{\Lambda}\text{He} + \alpha$ channel. The ground state of ${}^8\text{Be}$ subsystem is known to be a very narrow resonance just near 2α threshold. Hence space correlations between α -particles should also be considered properly. AMGOB model gives us a possibility to take into account two coupled binary cluster configurations ${}^5_{\Lambda}\text{He} + \alpha$ and ${}^8\text{Be} + \Lambda$ allowing for ${}^5_{\Lambda}\text{He}$ and ${}^8\text{Be}$ to be polarized. The term "cluster polarization" connotes changing energy of a two-cluster subsystem (and, hence, change of its shape and/or size) due to the interaction with the third cluster.

The light hypernuclei have been investigated within different models in Refs. [3–25]. In Ref. [7] $L^\pi = 0^+$ ground state and $L^\pi = 2^+$ excited states of ${}^9_{\Lambda}\text{Be}$ have been investigated with a microscopic cluster model. Spin of a Λ -hyperon was disregarded in [7] and, hence, all the states of ${}^9_{\Lambda}\text{Be}$ hypernucleus have been classified with the values of the total orbital momentum L . For the de-

scription of the core nucleus ${}^8\text{Be}$ the generator coordinate method of a microscopic 2α cluster model has been applied. The Λ -nucleus potentials have been constructed by folding ΛN interactions with the nuclear density calculated by the microscopic cluster model. A core polarization has been taken into account by artificial enhancing the central part of NN -potential. In this assumption, strengthening of the effective central nuclear interactions acts like an intensification of the inter-cluster potentials. This procedure simulates an additional attraction to the nuclear system from ΛN interaction. The optimum value of the enhancement factor was chosen to minimize the energy of the total system. Authors claimed that particularly remarkable core polarization effects are found in ${}^9_{\Lambda}\text{Be}$, because ${}^8\text{Be}$ is a very fragile system of the quasi-bound 2α state. The core polarization effects have been seen in the nuclear size change and the energy changes caused by the Λ -particle in ${}^9_{\Lambda}\text{Be}$. The significant shrinkage of 2α structure in ${}^9_{\Lambda}\text{Be}$ has also been reported.

In Ref. [26] energy spectra of bound and resonance states of ${}^9_{\Lambda}\text{Be}$ have been calculated within the framework of $\alpha + \alpha + \Lambda$ three-body model. The $\alpha - \alpha$ interaction was chosen so to reproduce the observed $\alpha - \alpha$ scattering phase shift and the ground state of ${}^8\text{Be}$ within the $\alpha - \alpha$ orthogonality condition model. The $\Lambda\alpha$ interaction was obtained by folding the ΛN interaction into the α cluster wave function. Even- and odd-states of ΛN interaction have been adjusted so as to reproduce the observed binding energies of the ground states in ${}^5_{\Lambda}\text{He}$ and ${}^9_{\Lambda}\text{Be}$. For the resonant states of ${}^9_{\Lambda}\text{Be}$ the complex scaling method has been employed. The level structure has been categorized into ${}^8\text{Be}$ -analogue states, genuine hypernuclear states, ${}^9\text{Be}$ analogue states, which have already been discussed in [27–29] and some new states located at more than 10 MeV above the $\alpha + \alpha + \Lambda$ threshold states.

An extensive discussion of the structure of genuine hypernuclear states of ${}^9_{\Lambda}\text{Be}$, as well as ${}^8\text{Be}^*$ -analogue states, within a microscopic $\alpha + \alpha(\alpha*) + \Lambda$ cluster model is given also in review paper [3].

In Ref. [30] ${}^9_{\Lambda}\text{Be}$ hypernucleus has been treated as the $S = 1/2$, $T = 0$ bound state of the three-cluster system $\alpha\alpha\Lambda$. The cluster-reduction method is used to solve the s-wave differential Faddeev equations. Phenomenological potentials have been used to describe $\Lambda\alpha$ and $\alpha\alpha$ interactions. The authors have considered boundary-value prob-

* ylashko@gmail.com

† nesterov@bitp.kiev.ua

‡ vsvasilevsky@gmail.com

lens corresponding to the bound states in the $\alpha\alpha\Lambda$ system and the problems of low-energy alpha-particle scattering on a ${}^5_{\Lambda}\text{He}$ hypernucleus. The s-wave phase shift for $\alpha-{}^5_{\Lambda}\text{He}$ scattering has been shown to behave anomalously at energies of relative motion below 1 MeV being small and positive. The scattering length has been observed to be large in magnitude and negative, which has been attributed by the authors to the presence of a virtual level in the $\alpha\alpha\Lambda$ system near the threshold for scattering.

In [31] the first ab initio calculations for p-shell single- Λ hypernuclei using no-core shell model approaches with explicit hyperons have been presented. In addition to chiral two- and three-nucleon interactions, they used leading-order (LO) chiral hyperon-nucleon (YN) interactions and a meson-exchange hyperon-nucleon interaction. They have shown that the chiral hyperon-nucleon interactions provide the ground-state and excitation energies that generally agree with experiment within the cutoff dependence. At the same time they demonstrated that hypernuclear spectroscopy provides tight constraints on the hyperon-nucleon interactions. A peculiarity of ${}^9_{\Lambda}\text{Be}$ is that the spin-doublet resulting from the 2^+ state in ${}^8\text{Be}$ is practically degenerate, with the higher J state being at slightly lower excitation energy experimentally, contrary to other light hypernuclei. The LO chiral YN interactions reproduce the excitation energy of the doublet and the near degeneracy within threshold extrapolation and convergence uncertainties. However, the order of levels is wrong. In contrast, the Julich'04 interaction [32] gives a significant splitting of the spin doublet in contradiction to experiment.

The energy splitting of the $5/2_1^+ - 3/2_1^+$ doublet states in ${}^9_{\Lambda}\text{Be}$, which was considered to be dominantly composed of the ${}^8\text{Be}(2_1^+) \otimes \Lambda(s_{1/2})$ configuration, has been studied in [12] within a microscopic three-body model $2\alpha + \Lambda$. The Pauli principle between two α clusters has been taken into account by the orthogonality condition model. The main purpose of Ref. [12] was to demonstrate how the splitting of the spin-doublet states in ${}^9_{\Lambda}\text{Be}$ is related to the underlying LS and antisymmetric LS forces (ALS), which are different between one-boson-exchange models and quark models. The quark model predicts that the ALS component of the LN interaction is so strong as to substantially cancel the LS one, while the one-boson-exchange models propose much smaller ALS and various strength of LS. The $\Lambda\alpha$ interactions are derived by folding the ΛN interaction into the density of the α cluster. The authors introduced a phenomenological ΛNN three-body force, folding of which leads to both $\Lambda\alpha\alpha$ and $\Lambda\alpha$ potentials. All the available Nijmegen one-boson-exchange model ΛN interactions lead to a wide range of splittings of 0.08-0.20 MeV in ${}^9_{\Lambda}\text{Be}$. At the same time, quark-model ΛN interactions, which have generally large ALS force, gives a half of the smallest one-boson-exchange model prediction for the splitting. These data are compatible with the experimental results reported in [13].

Based on the Faddeev methodology calculations of

$2\alpha + \Lambda$ system, which used two-cluster resonating-group method kernels, have been performed in Ref. [23]. The method, which was used in [23], is equivalent to the pairwise orthogonality condition model of three-cluster systems, interacting via two-cluster RGM kernels. The three-range Minnesota force, which describes the $\alpha\alpha$ phase shifts, has been chosen as an effective two-nucleon interaction. A simple two-range Gaussian potential for each spin-singlet and spin-triplet state, generated from the phase-shift behavior of the quark-model hyperon-nucleon interaction, has been used as a ΛN force for $\Lambda\alpha$ interaction. To solve the Faddeev equation, the authors discretized the continuous momentum variable for the Jacobi coordinate vectors. The authors stated that the $L^\pi = 0^+$ ground state and the $L^\pi = 2^+$ excited state of ${}^9_{\Lambda}\text{Be}$ are well described by the contracted 2α cluster structure with a weakly coupled Λ -particle in the dominant s-wave component. However, the energy gain for ${}^9_{\Lambda}\text{Be}$ due to partial waves higher than the s-wave is claimed to be about 1.2 MeV, because oscillatory behavior of the $\alpha\alpha$ relative wave functions needs more partial waves with a larger energy gain.

In the present paper the structure of bound and resonance states in ${}^9_{\Lambda}\text{Be}$ hypernucleus for the states $1/2 \leq J \leq 7/2$ of positive and negative parity is investigated with special emphasis on the impact of cluster polarization on the spectrum of the ${}^9_{\Lambda}\text{Be}$ and elements of scattering matrix. The Pauli exclusion principle between α -clusters is taken into account completely. We employ an effective ΛN single-channel interaction simulating the basic features of the Nijmegen meson-theoretical models NSC97f [12], in which a cut-off parameter k_F was adopted to reproduce the energy of the ground state of ${}^9_{\Lambda}\text{Be}$ with respect to $2\alpha + \Lambda$ threshold. As a NN interaction the modified Hasegawa-Nagata potential is chosen with the Majorana parameter being adjusted to give the experimentally observed energy of ${}^9\text{Be}$ nucleus. Parameters of resonance states are determined from analysis of the energy dependence of two-channel S -matrix for $\alpha-{}^5_{\Lambda}\text{He}$ and $\Lambda-{}^8\text{Be}$ scattering, provided that ${}^5_{\Lambda}\text{He}$ and ${}^8\text{Be}$ subsystems being in their ground states in entrance and exit channels.

The paper is organized as follows. Formulation of a microscopic three-cluster model used for the investigation of the ${}^9_{\Lambda}\text{Be}$ hypernucleus is given in Section II. In Section III we analyze how the spectrum of bound and resonance states of ${}^9_{\Lambda}\text{Be}$ depends on the polarization of two-cluster subsystems ${}^5_{\Lambda}\text{He}$ and ${}^8\text{Be}$. The nature of the obtained resonance states in ${}^9_{\Lambda}\text{Be}$ is also discussed in Section III. Conclusions are made in Section IV.

II. FORMULATION OF THE MODEL

Let us consider a microscopic Hamiltonian for a system consisting of 8 nucleons (two alpha-particles) and a Λ

hyperon:

$$\hat{H} = -\frac{\hbar^2}{2m} \sum_{i=1}^8 \frac{\partial^2}{\partial \mathbf{r}_i^2} - \frac{\hbar^2}{2m_\Lambda} \frac{\partial^2}{\partial \mathbf{r}_\Lambda^2} + \sum_{i<j}^8 V_{NN}(\mathbf{r}_i - \mathbf{r}_j) + \sum_{i=1}^8 V_{N\Lambda}(\mathbf{r}_i - \mathbf{r}_\Lambda) \quad (1)$$

where $m = (938.272 + 939.565)/2 = 938.919$ MeV/c² is a nucleon mass and $m_\Lambda = 1115.683(6)$ MeV/c² is a mass of the Λ hyperon. It is more expedient to use the mass of a nucleon m as a unit mass and than the mass of the hyperon $\bar{m}_\Lambda = m_\Lambda/m = 1.18826$. It is assumed that coordinates of nucleons and a coordinate of the hyperon are determined in the center-of-mass system, and thus center of mass motion is eliminated from the Hamiltonian.

The total Hamiltonian can be separated into nuclear and hypernuclear parts:

$$\hat{H} = \hat{H}_{NN} + \hat{H}_{N\Lambda},$$

$$\hat{H}_{NN} = -\frac{\hbar^2}{2m} \sum_{i=1}^8 \frac{\partial^2}{\partial \mathbf{r}_i^2} + \sum_{i<j}^8 V_{NN}(\mathbf{r}_i - \mathbf{r}_j), \quad (2)$$

$$\hat{H}_{N\Lambda} = -\frac{\hbar^2}{2m_\Lambda} \frac{\partial^2}{\partial \mathbf{r}_\Lambda^2} + \sum_{i=1}^8 V_{N\Lambda}(\mathbf{r}_i - \mathbf{r}_\Lambda). \quad (3)$$

Eigenfunctions of Hamiltonian (1) characterized with the total angular momentum J and energy E of the relative motion of the cluster will be sought in the form:

$$\Psi_{EJ} = \sum_L \sum_{\alpha=1}^2 \sum_{\lambda_\alpha, l_\alpha} \hat{\mathcal{A}} \{ \Phi_1(^4\text{He}) \Phi_2(^4\text{He}) \Phi_3(\Lambda) \} (4)$$

$$\times f_{\lambda_\alpha, l_\alpha; L}^{(E, J)}(x_\alpha, y_\alpha) \{ Y_{\lambda_\alpha}(\hat{\mathbf{x}}_\alpha) Y_{l_\alpha}(\hat{\mathbf{y}}_\alpha) \}_{LM} \}_{JM_J}.$$

Here we involve two Faddeev amplitudes $f_{\lambda_\alpha, l_\alpha; L}^{(E, J)}(x_\alpha, y_\alpha)$ which represent dynamics in binary channels ${}^5\text{He} + \alpha$ ($\alpha=1$) and ${}^8\text{Be} + \Lambda$ ($\alpha=2$). The Jacobi vector \mathbf{x}_1 ($=x_1 \cdot \hat{\mathbf{x}}_1$) determines distance between an alpha particle and a Λ hyperon:

$$\mathbf{x}_1 = \sqrt{\frac{4\bar{m}_\Lambda}{\bar{m}_\Lambda + 4}} \left[\mathbf{r}_\Lambda - \frac{1}{4} \sum_{i=1}^4 \mathbf{r}_i \right], \quad (5)$$

while the Jacobi vector \mathbf{y}_1 is the distance between an alpha particle and ${}^5\text{He}$ binary subsystem:

$$\mathbf{y}_1 = \sqrt{\frac{4(\bar{m}_\Lambda + 4)}{\bar{m}_\Lambda + 8}} \left[\frac{1}{4} \sum_{i=5}^8 \mathbf{r}_i - \frac{1}{\bar{m}_\Lambda + 4} \left(\mathbf{r}_\Lambda + \sum_{i=1}^4 \mathbf{r}_i \right) \right] \quad (6)$$

The second tree of Jacobi coordinates involves vector \mathbf{x}_2 , which describes the relative distance between two alpha particles,

$$\mathbf{x}_2 = \sqrt{2} \left[\frac{1}{4} \sum_{i=1}^4 \mathbf{r}_i - \frac{1}{4} \sum_{j=5}^8 \mathbf{r}_j \right] \quad (7)$$

and vector \mathbf{y}_2 , which determines position of the Λ -hyperon relative to the ${}^8\text{Be}$:

$$\mathbf{y}_2 = \sqrt{\frac{8\bar{m}_\Lambda}{\bar{m}_\Lambda + 8}} \left[\mathbf{r}_\Lambda - \frac{1}{8} \sum_{i=1}^8 \mathbf{r}_i \right] \quad (8)$$

It is worthwhile underlining that the antisymmetrization operator $\hat{\mathcal{A}}$ in (4) permutes coordinates of nucleons only. It does not involve a hyperon. Due to this fact, in the second Jacobi tree adopted for describing the channel ${}^8\text{Be} + \Lambda$ we have got a folding type of function Ψ_{EJ} in (4) with the wave function of ${}^8\text{Be}$ being antisymmetric. In the first Jacobi tree associated with the channels ${}^5\text{He} + \alpha$ the antisymmetrization operator $\hat{\mathcal{A}}$ invokes the exchange of nucleons between ${}^5\text{He}$ and an alpha particle and thus makes antisymmetric a wave function of the compound system ${}^9\text{Be}$.

Equation (4) represents the wave function in the LS coupling scheme. Partial orbital momentum λ_α indicates an internal orbital momentum of ${}^5\text{He}$ ($\alpha=1$) or ${}^8\text{Be}$ ($\alpha=2$), while orbital momentum l_α describes rotation of an alpha particle around ${}^5\text{He}$ ($\alpha=1$) or rotation of the Λ -hyperon around ${}^8\text{Be}$ ($\alpha=2$). The total orbital momentum L is a vector sum of partial orbital momenta: $\vec{L} = \vec{\lambda}_\alpha + \vec{l}_\alpha$. Since the spins of alpha-clusters are equal to zero, the total spin of the hypernucleus ${}^9\text{Be}$ is determined by the spin of the Λ -hyperon and equals 1/2. Thus with a given value of the total angular momentum J the total orbital momentum L can have two values $L = J - 1/2$ and $L = J + 1/2$. It is true for all values of J and parity π except when $J^\pi = 1/2^-$ where the total orbital momentum has only one value $L = 1$.

Faddeev three-cluster amplitudes $f_{\lambda_\alpha, l_\alpha; L}^{(E, J)}(x_\alpha, y_\alpha)$ are the solutions of an infinite set of integro-differential equations resulting from Schrödinger equation for the wave function (4) with the Hamiltonian (1):

$$\begin{aligned}
& \left[\widehat{T}_{x_\alpha, l_\alpha} + \widehat{T}_{y_\alpha, l_\alpha} - E \right] f_{\lambda_\alpha, l_\alpha; L}^{(E, J)} (x_\alpha, y_\alpha) \\
& + \sum_{\beta=1}^2 \sum_{\lambda_\beta, l_\beta} \int_0^\infty \int_0^\infty d\tilde{x}_\beta \tilde{x}_\beta^2 d\tilde{y}_\beta \tilde{y}_\beta^2 \mathcal{V}_{\lambda_\alpha, l_\alpha; \lambda_\beta, l_\beta}^{(L)} (x_\alpha, y_\alpha; \tilde{x}_\beta, \tilde{y}_\beta) \cdot f_{\lambda_\beta, l_\beta; L}^{(E, J)} (\tilde{x}_\beta, \tilde{y}_\beta) \\
& = E \sum_{\beta=1}^2 \sum_{\lambda_\beta, l_\beta} \int_0^\infty \int_0^\infty d\tilde{x}_\beta \tilde{x}_\beta^2 d\tilde{y}_\beta \tilde{y}_\beta^2 \mathcal{N}_{\lambda_\alpha, l_\alpha; \lambda_\beta, l_\beta}^{(L)} (x_\alpha, y_\alpha; \tilde{x}_\beta, \tilde{y}_\beta) \cdot f_{\lambda_\beta, l_\beta; L}^{(E, J)} (\tilde{x}_\beta, \tilde{y}_\beta),
\end{aligned} \tag{9}$$

where

$$\widehat{T}_{z, l} = -\frac{\hbar^2}{2m} \left[\frac{d^2}{dz^2} + \frac{2}{z} \frac{d}{dz} - \frac{l(l+1)}{z^2} \right]$$

is the kinetic energy operator associated with the Jacobi vector $\mathbf{z} = \mathbf{x}_\alpha$ or $\mathbf{z} = \mathbf{y}_\alpha$, $\mathcal{N}_{\lambda_\alpha, l_\alpha; \lambda_\beta, l_\beta}^{(L)}$ is the exchange part of the norm kernel, and $\mathcal{V}_{\lambda_\alpha, l_\alpha; \lambda_\beta, l_\beta}^{(L)}$ contains a direct and an exchange part of the potential energy and an exchange term of the kinetic energy of the three-cluster system.

We can reduce a three-cluster problem to a many-channel two-body problem by expanding the wave function $f_{\lambda_\alpha, l_\alpha; L}^{(E, J)} (x_\alpha, y_\alpha)$ into the basis of eigenfunctions of the two-cluster Hamiltonian consisting of bound states $g_{\mathcal{E}_\alpha^\sigma \lambda_\alpha} (x_\alpha)$ ($\sigma = 1, 2, \dots$) and continuous spectrum states $g_{\mathcal{E}_\alpha \lambda_\alpha} (x_\alpha)$:

$$\begin{aligned}
f_{\lambda_\alpha, l_\alpha; L}^{(E, J)} (x_\alpha, y_\alpha) &= \sum_{\sigma} g_{\mathcal{E}_\alpha^\sigma \lambda_\alpha} (x_\alpha) \cdot \phi_{E - \mathcal{E}_\alpha^\sigma, l_\alpha} (y_\alpha) \tag{10} \\
&+ \int d\mathcal{E}_\alpha g_{\mathcal{E}_\alpha \lambda_\alpha} (x_\alpha) \phi_{E - \mathcal{E}_\alpha, l_\alpha} (y_\alpha).
\end{aligned}$$

Functions $g_{\mathcal{E}_\alpha^\sigma \lambda_\alpha} (x_\alpha)$ and $g_{\mathcal{E}_\alpha \lambda_\alpha} (x_\alpha)$ satisfy the two-cluster Schrödinger equation:

$$\begin{aligned}
& \left[\widehat{T}_{x_\alpha, l_\alpha} - \mathcal{E}_\alpha \right] g_{\mathcal{E}_\alpha \lambda_\alpha} (x_\alpha) \tag{11} \\
& + \int_0^\infty d\tilde{x}_\alpha \tilde{x}_\alpha^2 \cdot \mathcal{V}^{(\lambda_\alpha)} (x_\alpha; \tilde{x}_\alpha) \cdot g_{\mathcal{E}_\alpha \lambda_\alpha} (\tilde{x}_\alpha) \\
& = \mathcal{E}_\alpha \int_0^\infty d\tilde{x}_\alpha \tilde{x}_\alpha^2 \cdot \mathcal{N}^{(\lambda_\alpha)} (x_\alpha; \tilde{x}_\alpha) \cdot g_{\mathcal{E}_\alpha \lambda_\alpha} (\tilde{x}_\alpha).
\end{aligned}$$

Functions $\phi_{E - \mathcal{E}_\alpha^\sigma, l_\alpha} (y_\alpha)$ and $\phi_{E - \mathcal{E}_\alpha, l_\alpha} (y_\alpha)$ describe scattering of the third cluster on a two-cluster bound state with energy $\mathcal{E}_\alpha^\sigma$ or a continuum spectrum state with energy \mathcal{E}_α , correspondingly. Quantities $\mathcal{N}^{(\lambda_\alpha)} (x_\alpha; \tilde{x}_\alpha)$ and $\mathcal{V}^{(\lambda_\alpha)} (x_\alpha; \tilde{x}_\alpha)$ have the same meaning as the similar quantities in Eq. (9), but for two-cluster systems.

So, first we solve two-cluster equation (11) and then use the eigenfunctions of the two-cluster Hamiltonian to find wave functions $\phi_{E - \mathcal{E}_\alpha^\sigma, l_\alpha} (y_\alpha)$ and $\phi_{E - \mathcal{E}_\alpha, l_\alpha} (y_\alpha)$. Finally, we get three-cluster wave function $f_{\lambda_\alpha, l_\alpha; L}^{(E, J)} (x_\alpha, y_\alpha)$.

In practical calculations the integral part of the expansion (10) is substituted with the sum over the finite number of the discretized states in two-cluster continuum. The more terms in this sum are, the better cluster polarization is taken into account.

As in [2], we use a finite number of square-integrable Gaussian functions to expand two-cluster wave function $g_{\mathcal{E} \lambda_\alpha} (x_\alpha)$:

$$g_{\mathcal{E} \lambda_\alpha} (x_\alpha) = \sum_{\nu=1}^{N_G^{max}} D_\nu^{(\mathcal{E} \lambda_\alpha)} G_{\lambda_\alpha} (x_\alpha, b_\nu), \tag{12}$$

where

$$\begin{aligned}
G_\lambda (\mathbf{x}, b_\nu) &= \sqrt{\frac{2}{b_\nu^3 \Gamma(\lambda_\alpha + 3/2)}} \rho^{\lambda_\alpha} \exp \left\{ -\frac{1}{2} \rho^2 \right\}, \tag{13} \\
\rho &= \frac{x}{b_\nu}
\end{aligned}$$

is a Gaussian function. Parameters b_ν are chosen so to minimize the ground state energies of the two-body subsystems.

To find wave functions $\phi_{E - \mathcal{E}, l_\alpha} (y_\alpha)$ of the third cluster interacting with the two-cluster subsystem numerated by index α ($\alpha = 1, 2$), we expand them over the oscillator basis

$$\phi_{E - \mathcal{E}, l_\alpha} (y_\alpha) = \sum_{n_\alpha=0}^{N_0-1} C_{n_\alpha}^{(E - \mathcal{E}, l_\alpha)} \psi_{n_\alpha, l_\alpha} (y_\alpha, b), \tag{14}$$

where

$$\begin{aligned}
\psi_{n_\alpha, l_\alpha} (y_\alpha, b) &= (-1)^{n_\alpha} \mathcal{N}_{n_\alpha l_\alpha} \tilde{\rho}^{l_\alpha} e^{-\frac{1}{2} \tilde{\rho}^2} L_{n_\alpha}^{l_\alpha+1/2} (\tilde{\rho}^2), \tag{15} \\
\tilde{\rho} &= \frac{y_\alpha}{b}, \quad \mathcal{N}_{n_\alpha l_\alpha} = \sqrt{\frac{2 \Gamma(n_\alpha + 1)}{b^3 \Gamma(n_\alpha + l_\alpha + 3/2)}}
\end{aligned}$$

is an oscillator function and b is the oscillator length.

In eq. (14), a finite number of oscillator functions appears. But in fact, this expansion involves an infinite number of functions, since we know an asymptotic behavior of wave function $\phi_{E - \mathcal{E}, l_\alpha} (y_\alpha)$ in coordinate space and expansion coefficients $C_{n_\alpha}^{(E - \mathcal{E}, l_\alpha)}$ in oscillator space.

At large distances $x_1 \ll y_1$ between an α -particle and a ${}^3\text{He}$ subsystem being in the state with energy \mathcal{E}_1 wave function $\phi_{E - \mathcal{E}_1, l_1} (y_1)$ has the following form:

$$\phi_{E - \mathcal{E}_1, l_1} (y_1) \approx \delta_{c_0, c} \psi_{l_1}^{(-)} (k_1 y_1; \eta_1) - S_{c_0, c} \psi_{l_1}^{(+)} (k_1 y_1; \eta_1), \tag{16}$$

where $S_{c_0, c}$ is the scattering matrix, index c numerates an exit channel $c = \{\mathcal{E}_1 \lambda_1 l_1\}$ and c_0 indicates the entrance channel, $\psi_{l_1}^{(-)} (\psi_{l_1}^{(+)})$ is the incoming (outgoing) Coulomb wave, and η_1 is Sommerfeld parameter. Determination

of the incoming and outgoing Coulomb wave functions can be found, for instance, in Ref. [33].

The asymptotic behaviour of the wave function $\phi_{E-\mathcal{E}_2, l_2}(y_2)$ describing scattering of a Λ -hyperon on ^8Be subsystem being in the state with energy \mathcal{E}_2 is determined by a superposition of the Hankel functions $H_{l_2+1/2}^{(\pm)}$, since Λ -hyperon does not have an electric charge:

$$\phi_{E-\mathcal{E}_2, l_2}(y_2) \approx \delta_{c_0, c} H_{l_2+1/2}^{(-)}(k_2 y_2) - S_{c_0, c} H_{l_2+1/2}^{(+)}(k_2 y_2), \quad (17)$$

Parameters $k_{1,2}$ and η_1 in our case are defined as

$$k_{1,2} = \sqrt{\frac{2m(E - \mathcal{E}_{1,2})}{\hbar^2}},$$

$$\eta_1 = \frac{Z^2 e^2}{\sqrt{2(E - \mathcal{E}_{1,2})}} \sqrt{\frac{m}{\hbar^2} \frac{4(4 + \bar{m}_\Lambda)}{\bar{m}_\Lambda + 8}},$$

where $Z = 2$ is a charge of α -cluster, E is the total energy of three-cluster system ($E > \mathcal{E}_{1,2}$).

For numerical investigations of the three-cluster system $^9\Lambda\text{Be}$, we have to use a finite basis of Gaussian and oscillator functions. As was pointed out above, N_G^{\max} Gaussian functions give us the same number of eigenstates and corresponding eigenfunctions of a two-cluster Hamiltonian. To study effects of cluster polarization, we will involve different numbers of these eigenstates, their actual number we denote as N_G ($1 \leq N_G \leq N_G^{\max}$).

Index N_f numerates a cumulative number of a basis function for the σ_α th eigenstate of the α th ($\alpha=1, 2$) two-cluster subsystem with energy $\mathcal{E}_{\sigma_\alpha}$ ($1 \leq \sigma_\alpha \leq N_G$) and for n_α oscillator quanta ($0 \leq n_\alpha \leq N_O - 1$):

$$N_f = 1 + n_\alpha + (\sigma_\alpha - 1) N_O + (\alpha - 1) N_G N_O, \quad (18)$$

$$1 \leq N_f \leq 2N_G N_O.$$

Thus, in our calculations we deal with the $2N_G$ -channel system for the case of two coupled binary configurations. In an isolated configuration approximation the number of channels equals N_G .

Traditionally, the spectrum of the bound states is obtained with the diagonalization of the three-cluster Hamiltonian with N_f basis functions. The diagonalization also reveals a large numbers of pseudo-bound states which are specific combinations of scattering states. In what follows, we are going to study both bound and pseudo-bound states.

To obtain scattering wave functions and elements of scattering S -matrix, we will solve a system of nonhomogeneous algebraic equations for the expansion coefficients. For scattering states, the number of oscillator functions N_O determines a border between an internal and asymptotic regions. It is obvious that the number of channels and the number of basis functions can be different for calculating bound and scattering states.

III. RESULTS AND DISCUSSIONS

In the present paper we restrict the discussion to the case of zero orbital momenta λ_α of binary subsystems $^5\Lambda\text{He}$ and ^8Be . Hence, orbital momentum l_α describing relative motion of the binary subsystems and the third cluster determines the total orbital momentum $L = l_\alpha$ and parity. Consequently, a state with a given total angular momentum and parity J^π corresponds to the only value of L . Namely, positive parity states are characterized by even values of L , while negative parity states correspond to the odd values of L . $J^\pi = 1/2^+$ states have zero total orbital momentum.

In the asymptotic region we have taken into account two channels describing the scattering of an α -particle on $^5\Lambda\text{He}$ subsystem and a Λ -hyperon on ^8Be subsystem, provided that both subsystems are in their ground states. In the internal region three more excited states for each subsystem have also been considered. Such an approximation allows for polarization of two-cluster subsystems due to the interaction with the third cluster at small distances between clusters, but at large distances binary subsystems can be only in their ground states.

A. Input parameters

First of all we need to select values for the input parameters. We involve the modified Hasegawa-Nagata (MHNP) [34, 35] potential as a nucleon-nucleon interaction. We use the same nucleon-hyperon potential as in Ref. [36]. Parameters of the spin-orbit interaction of the ΛN interaction are taken for the version NSC97f from Ref. [12]. In Fig. 1 we display the even components of the nucleon-hyperon potential.

Traditionally we chose the oscillator length $b = 1.317$ fm to minimize the threshold energy of the two-cluster subsystems. The value $m = 0.0332$ of Majorana parameter of the MHNP is adjusted to reproduce the energy and width of the ground state in ^9Be nucleus relative to $\alpha + \alpha + n$ threshold. Cut-off parameter $k_{\text{eff}} = 0.889$ fm $^{-1}$ of the ΛN -potential is selected to reproduce the energy of the ground state of $^9\Lambda\text{Be}$ nucleus with respect to $\alpha + \alpha + \Lambda$ threshold.

Parameters b_ν ($\nu = \overline{1, 4}$) of Gaussian functions are determined as $b_\nu = b_0 q^{\nu-1}$. For $^5\Lambda\text{He}$ we selected $b_0 = 0.7$ fm, $q = 1.85$, and for ^8Be we took $b_0 = 1.15$ fm, $q = 2.2$. Such values of the parameters minimize the ground state energies of the $^5\Lambda\text{He}$ and ^8Be nuclei.

B. Spectrum of $^9\Lambda\text{Be}$ nucleus

1. Convergence of parameters of resonance states

The spectrum of positive and negative parity states for $1/2 \leq J \leq 7/2$ of the $^9\Lambda\text{Be}$ nucleus calculated within the AMGOB model is presented in Tables I, II. Tables I,

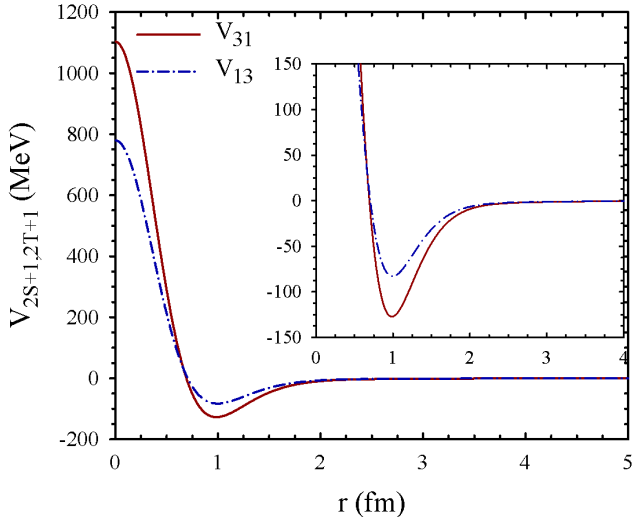


FIG. 1. The even components of the central part of the NA potential.

II demonstrate that the polarization of two-cluster subsystems plays an important role in formation of bound and resonance states of the ${}^9\Lambda\text{Be}$. For the positive parity states, cluster polarization decreases energy of the bound and resonance states. It also reduces significantly total width of the resonance states. Cluster polarization, for example, decreases the energy of the ${}^9\Lambda\text{Be}$ ground $1/2^+$ state by 400 keV, and the energy of the $3/2_1^+$ resonance state which determined in experiments as the second excited state is reduced by 245 keV, while its total width decreases more than 6 times. Similar situation with the $5/2_1^+$ resonance state which has approximately the same energy. Cluster polarization shifts down the energy of the resonance state by 302 keV and causes an eightfold decrease in its width. Besides, allowing for polarization leads to the formation of a large number of narrow resonance states in three-cluster continuum above the decay threshold ${}^9\Lambda\text{Be} \Rightarrow {}^8\text{Be}(0_2^+) + \Lambda$ located at 1.63 MeV above the three-cluster decay threshold.

For the negative parity states we observe from Table II that the parameters of the lowest $1/2_1^-$ and $3/2_1^-$ resonance states remain almost intact when cluster polarization is taken into account. The energy of this resonance is quite close to the energy 0.7 MeV where becomes possible ${}^8\text{Be}(0_1^+) + \Lambda$ scattering. Since the latter channel is considered properly already in the approximation of rigid two-cluster subsystems, allowing for cluster polarization does not change a lot the lowest $1/2_1^-$ and $3/2_1^-$ states. It might be well to point out that spectra of the $1/2^-$ and $3/2^-$ states are almost degenerate, because they are characterized by the same orbital momentum $L = 1$ and the spin-orbit interaction is small.

Analyzing partial widths of the resonance states tabulated in Tables I and II we can observe that the majority

TABLE I. Spectrum of positive parity states of ${}^9\Lambda\text{Be}$ nucleus obtained within the AMGOB model. Γ is a total width of the resonance state, $\Gamma_{1,2}$ are partial decay widths of the resonance via ${}^5\text{He} + \alpha$ and ${}^8\text{Be} + \Lambda$ channels, correspondingly. Energy is given in MeV, the total and partial widths are in keV.

J^π	E	rigid			soft			
		Γ	Γ_1	Γ_2	E	Γ	Γ_1	Γ_2
$1/2^+$	-6.204				-6.623			
	5.360	3170	170	3000	1.792	3.3	2.3	1
					2.252	60.3	11.8	48.5
					2.733	384	0.6	383.4
					3.396	349.2	84.6	264.6
					4.107	213.6	23.3	190.3
					4.650	470.8	77.8	393
					5.083	10.8	8.4	2.4
$3/2^+$	-3.297	35.8	35.8		-3.543	5.5	5.5	
					2.115	0.045	0.01	0.035
					2.850	0.027	0.01	0.017
					3.314	206.9	0.1	206.8
					3.886	8.3	2	6.3
					4.387	105.7	1.6	104.1
					5.212	26.2	4.3	21.9
					5.610	55.8	0.4	55.4
$5/2^+$	-3.446	12	12		-3.748	0.75	0.75	
					2.115	0.043	0.01	0.033
					2.849	0.041	0.037	0.004
					3.312	210.42	0.07	210.35
					3.885	8.3	2	6.3
					4.386	107.8	1.3	106.5
					5.209	26.7	4.2	22.5
					5.630	57.64	0.17	57.4
$7/2^+$	4.726	2962.5	2962.4	0.1	2.610	0.0091	0.0088	0.0003
					3.643	0.002	0.0007	0.0013
					3.979	8.302	0.001	8.301
					4.500	2625.2	2625.2	0.01
					5.139	1.6	0.09	1.51

of the resonances decay via ${}^8\text{Be} + \Lambda$ channel. There are not more than 2 resonances decaying via ${}^5\text{He} + \alpha$ channel for a given value of J^π . In all the cases, except $5/2_6^-$ and $7/2_6^-$ resonances, partial widths via different channels significantly differ from one another. The above mentioned $5/2_6^-$ and $7/2_6^-$ states represent the only case when the resonances decay with almost equal probability via both channels. It is interesting to note also the principal change in partial widths of the lowest $1/2_1^+$ resonance. Allowing for cluster polarization not only halves the energy of this resonance state, but also changes its dominant decay channel.

In the energy region considered $E \leq 6$ MeV above $2\alpha + \Lambda$ threshold four open channels could play a part in the formation of resonance states. They correspond to $\sigma = 1, 2$ eigenstates of the two-cluster subsystems calculated with four Gaussian functions and listed in Table III. We can assume that appearance of narrow resonances in the case when cluster polarization is taken into account could result from coupling the channels belonging to the same cluster configuration: ${}^8\text{Be}(0_1^+) + \Lambda$ and ${}^8\text{Be}(0_2^+) + \Lambda$

TABLE II. Spectrum of negative parity states of ${}^9\Lambda$ Be nucleus obtained within the AMGOB model. Γ is a total width of the resonance state, $\Gamma_{1,2}$ are partial decay widths of the resonance via ${}^5\Lambda$ He+ α and ${}^8\text{Be}+\Lambda$ channels, correspondingly. Energy is given in MeV, the total and partial widths are in keV.

J^π	E	rigid		soft		Γ_1	Γ_2	
		Γ	Γ_1	Γ_2	E			
$1/2^-$	0.723	4521	0.4	4520.6	0.724	4228.5	0.4	4228.1
					1.924	3.74	3.735	0.005
					2.519	30.1	21.1	9
					3.364	259.3	72.5	186.8
					4.350	250.8	0.1	250.7
					5.739	148.4	1.2	147.2
					5.906	91.3	2.9	88.4
					3/2 ⁻	4507.4	0.4	4507
					0.724	4213.7	0.5	4213.2
					1.924	3.99	3.97	0.02
$5/2^-$	5/2 ⁻	2.345	0.132	0.003	0.129	3.227	0.1157	0.0007
$7/2^-$	7/2 ⁻	2.345	0.145	0.001	0.144	3.227	0.197	0.001

channels, ${}^5\Lambda$ He(0_1^+) + α and ${}^5\Lambda$ He(0_2^+) + α channels. In particular, the first pair of the channels could be more coupled due to proximity of the energies needed to make the channels open.

Referring to Table III it will be observed that in our model ${}^5\Lambda$ He subsystem is overbound by 0.9 MeV compared to its experimental binding energy. However, this overbinding is much smaller than in other simple model calculations based upon ΛN potentials [37].

In Table III we also display the mass root-mean-square radius for all bound and pseudo-bond states. As we see, the ground state of ${}^5\Lambda$ He is a compact two-cluster system, while the lowest pseudo-bound state, representing the ground state of ${}^8\text{Be}$, is very dispersed with the large value of $r_m = 5.71$ fm. Dispersed are also states $\sigma = 2$ and $\sigma = 3$ of ${}^8\text{Be}$ and the state $\sigma = 2$ of ${}^5\Lambda$ He, however with the smaller values of r_m .

Table III shows also the average distances \bar{r}_α between clusters. They are determined in the following way

$$\bar{r}_\alpha = b \sqrt{\langle g_{\mathcal{E}_\sigma, \lambda_\alpha} | x_\alpha^2 | g_{\mathcal{E}_\sigma, \lambda_\alpha} \rangle / \mu_\alpha},$$

where μ_α is a reduced mass appearing in the definition of the Jacobi vector \mathbf{x}_α . The quantity \bar{r}_α gives the most

TABLE III. Energy and mass root-mean-square radius of the two-cluster bound and pseudo-bound states. The energy is measured from a two-cluster threshold indicated in the first column.

2C-system	Quantity	$\sigma = 1$	$\sigma = 2$	$\sigma = 3$	$\sigma = 4$
${}^5\Lambda$ He= $\alpha + \Lambda$	E , MeV	-4.06	2.91	21.12	139.76
	r_m , fm	1.71	3.25	2.20	1.48
	\bar{r}_α , fm	2.62	6.72	4.06	1.78
${}^8\text{Be}= \alpha + \alpha$	E , MeV	0.70	1.63	9.11	53.03
	r_m , fm	5.71	4.37	3.05	1.95
	\bar{r}_α , fm	15.16	7.07	2.34	1.39

probable relative distance between the interacting clusters. This quantity has been discussed in the literature. For example, in Ref. [7] devoted to the study of spectrum of p -shell hypernuclei including ${}^9\Lambda$ Be within a microscopic cluster model, the average distance between two alpha particles in the ground state of ${}^8\text{Be}$ were determined approximately. It was obtained that $\bar{r}_\alpha = 5.99$ fm which is smaller than our estimation $\bar{r}_\alpha = 15.16$ fm. We believe that such a large difference for the average distance between alpha particles can be partially ascribed to different nucleon-nucleon potentials involved in Ref. [7] and in our calculations. But the main difference is related to the way how this quantity is determined. Note that detail investigation of the average distance between two alpha particles in different states of ${}^8\text{Be}$ has been performed in Ref. [38] within the two-cluster resonating group method.

2. Spectrum of the $3/2^+$ states

In Fig. 2 we display the spectrum of the Hamiltonian for the $3/2^+$ states. The spectrum is obtained in a single-configuration (SC) and coupled-configuration (CC) approximations. Eigenvalues of the Hamiltonian are shown as a function of the number of basis functions N_f defined by Eq. (18). It is necessary to recall that in the present calculations the single-configuration approximation involves four different channels with a binary subsystem in the ground and three excited states. 200 oscillator functions are employed in each channel. Thus the region $1 \leq N_f \leq 800$ in both panels of Fig. 2 corresponds to the SC approximation, and the region $801 \leq N_f \leq 1600$ represents the CC approximation. The range $1 \leq N_f \leq 200$ shows the spectrum of eigenstates created by basis functions of the channel ${}^5\Lambda$ He(0_1^+) + α (left panel) and ${}^8\text{Be}(0_1^+) + Λ (right panel), the range $201 \leq N_f \leq 400$ display effects on the eigenspectrum of the second channel ${}^5\Lambda$ He(0_2^+) + α and ${}^8\text{Be}(0_2^+) + Λ , correspondingly, and so on.$$

One can see that there are a large number of plateaus which appear in the SC and CC approximations. The dot-dashed lines indicate the position of the $3/2^+$ resonance states, obtained by solving the dynamic equations

with proper boundary conditions. Such a plateau can be a marker of a narrow resonance state in the system under consideration. Besides, in many-channel systems the plateaus may appear due to a weak coupling of channels. It is worthwhile noticing that the second type of plateau may appear, for example, when a weak spin-orbit interaction couples states with different values of the total orbital momentum L and/or total spin S (LS coupling scheme).

Many plateaus which are observed in Fig. 2 in the single-configuration approximations belong to the second type. Indeed, if we have a closer look at the spectrum we can see that the channel describing the interaction of the third cluster with the most compact two-cluster subsystem (${}^5_{\Lambda}\text{He}(0_1^+) + \alpha$ or ${}^8\text{Be}(0_1^+) + \Lambda$) is dominant and noticeably reduces the energy of the eigenstates. Second in importance to the eigenstates of the ${}^9_{\Lambda}\text{Be}$ hypernucleus are ${}^5_{\Lambda}\text{He}(0_2^+) + \alpha$ and ${}^8\text{Be}(0_2^+) + \Lambda$ channels. All other channels are weakly coupled to the dominant channels and thus contribute much less to the energy of the eigenstates shown in Fig. 2. The same is also valid for a number of plateaus occurring in the CC area. We can also see in Fig. 2 that in many cases the energy of resonance states is close to the energy of plateau. The narrower is a resonance state, the closer is its energy to the plateau energy.

TABLE IV. Spectrum of $J^\pi = 3/2^+$ states of ${}^9_{\Lambda}\text{Be}$ nucleus obtained within the AMGOB model for different degree of polarization of two-cluster subsystems. Energy is in MeV and width is in keV.

$N_G = 1$		$N_G = 2$		$N_G = 3$		$N_G = 4$	
E	Γ	E	Γ	E	Γ	E	Γ
-3.297	35.8	-3.430	13.9	-3.539	5.6	-3.543	5.5
		2.115	0.08	2.115	0.08	2.115	0.04
		2.850	0.125	2.850	0.02	2.850	0.03
		3.319	197.6	3.314	206.9	3.3136	206.9
		3.887	9.4	3.886	8.3	3.886	8.3
		4.387	104.5	4.387	105.7	4.387	105.7
		5.217	32.1	5.212	26.2	5.212	26.2
		5.643	68.6	5.630	55.8	5.630	55.8

As Table IV suggests, the qualitative change of the spectrum is caused by taking into account the 0_2^+ state in ${}^5_{\Lambda}\text{He}$ and ${}^8\text{Be}$ subsystem. Allowing for higher excited states leads only to some slight alteration of energies and widths, but does not change the number of resonances. From this fact, we might reason that 0_2^+ states of the binary subsystems plays a large part in the structure of resonance states of ${}^9_{\Lambda}\text{Be}$ nucleus.

In Table V we compare spectrum of the $3/2^+$ resonance states obtained with and without Coulomb forces. 200 oscillator functions are used in both calculations. The results presented in Table V allow us to reveal effects of the Coulomb forces on energy and width of the resonance states in ${}^9_{\Lambda}\text{Be}$, and to understand peculiarities of the present model. We can conclude from Table V that without the Coulomb forces energy of all the resonance

TABLE V. Effects of the Coulomb forces on the energy and width of the $3/2^+$ resonance states.

with Coulomb		without Coulomb	
E , MeV	Γ , keV	E , MeV	Γ , keV
-3.543	5.5	-5.103	0
2.115	0.04	1.129	1.122
2.850	0.03	1.865	0.107
3.314	206.9	2.764	29.034
3.886	8.3	3.126	64.264

states is decreased by approximately 1 MeV, and the lowest $3/2_1^+$ resonance state with $E = -3.542$ MeV below the three-cluster threshold is transformed into a bound state. It is interesting to note that the Coulomb interaction makes $3/2_4^+$ resonance state wider and other resonance states narrower.

Figure 3 illustrates the behaviour of the phase shifts of elastic scattering for $J^\pi = 3/2^+$ states of ${}^9_{\Lambda}\text{Be}$ hypernucleus. We can observe from Fig. 3 a large impact of cluster polarization on the phase shifts of elastic scattering. It is interesting to note that the phase shift of ${}^5_{\Lambda}\text{He}(0_1^+) + {}^4\text{He}$ scattering manifests resonance behaviour only for the lowest $3/2_1^+$ state and the $3/2_4^+$. All other resonances become apparent only in the behaviour of ${}^8\text{Be}(0_1^+) + \Lambda$ scattering phase.

3. Comparison with other methods and experiment

In Table VI we display the spectrum of ${}^9_{\Lambda}\text{Be}$ obtained in Refs. [39] and [40], and compare it with our results. As this nucleus has not more than two bound states and

TABLE VI. Spectrum of bound and resonance states in ${}^9_{\Lambda}\text{Be}$ obtained in different models. Energy is displayed in MeV.

[39]			Present Method			[40]		
L^π	E	Γ , MeV	J^π	E	Γ , keV	J^π	E	Γ , MeV
0_1^+	-6.65	-	$1/2_1^+$	-6.62	-	$1/2_1^+$	-7.13	
2_1^+	-3.82	-	$5/2_1^+$	-3.75	0.75	$3/2_1^+$	-3.89	
1_1^-	0.1	2.5	$3/2_1^+$	-3.54	5.5	$5/2_1^+$	-3.89	
4_1^+	3.2	0.78	$1/2_2^+$	1.79	3.3	$3/2_1^-$	-2.94	0.12
3_1^-	8.0	6.1	$1/2_1^-$	1.92	3.7	$3/2_2^-$	-2.21	2.16
4_1^-	10.0	10.4	$3/2_1^-$	1.92	4.0	$3/2_3^-$	3.86	0.0056
			$7/2_1^+$	2.61	0.009			

a large number of resonance states, we selected those investigations which determined both energies and widths of the excited states.

In Ref. [39] a three-cluster model with an approximate treatment of the Pauli principle was employed. The $\alpha\Lambda$ interaction was determined in a folding approximation with the same ΛN potential as in the present paper, however another value of the parameter k_F ($k_F = 0.963$ fm $^{-1}$) was selected. The complex scaling method was

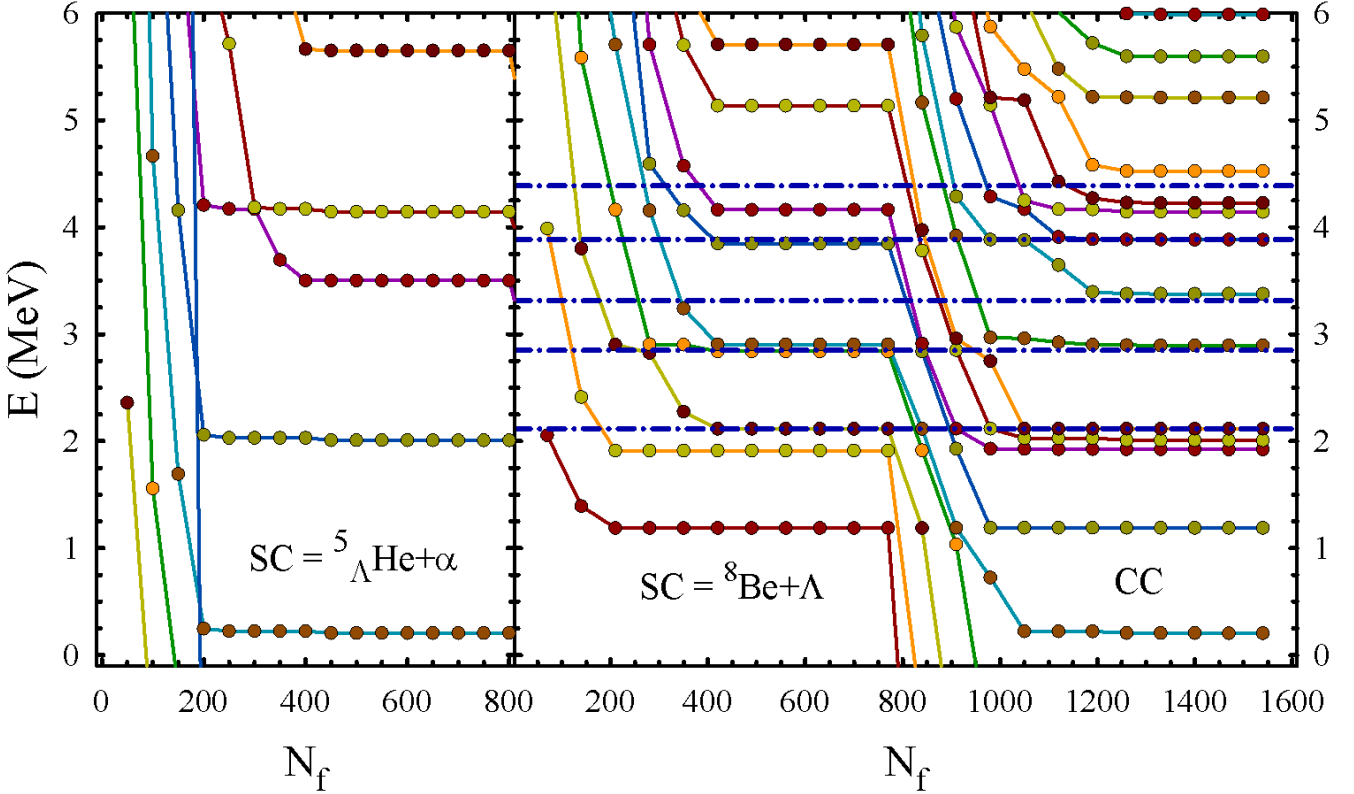


FIG. 2. Spectrum of eigenstates of the internal part of Hamiltonian for $3/2^+$ states constructed in a single-configuration (SC) and coupled-configuration (CC) approximations. The $3/2^+$ resonance states are displayed by the dot-dashed line in the area of the CC approximation. Energy is measured from the three-cluster decay threshold $\alpha + \alpha + \Lambda$.

involved in Ref. [39] to locate the energy and width of resonance states.

As the spin-orbit interaction is disregarded in Ref. [39], the authors labelled the states of the ${}^9\Lambda\text{Be}$ with the total orbital momentum L . The energy of the ground state, obtained in Ref. [39] is close to our results. There is also a certain likeness of our results and the results of Ref. [39] for the energy of the 2_1^+ state. However, in our approach this state is split by spin-orbit interaction on two states - $5/2_1^+$ and $3/2_1^+$, and these states are resonances, since in our calculations they are located above the lowest ${}^5\Lambda\text{He}(0_1^+) + \Lambda$ threshold. An important point is that our model reproduce the correct order of the $5/2_1^+$ and $3/2_1^+$ states and only slightly overestimates their splitting.

There is a dramatic difference in the position of other resonance states and, especially, in the widths of resonances. The resonance states obtained in Ref. [39] are very wide with the widths within the range $0.78 \leq \Gamma \leq 10.4$ MeV, while the resonance states obtained with our approach and listed in Table VI are very narrow ($0.009 \leq \Gamma \leq 5.5$ keV). As for the complete list of the resonance states collected in Tables I and II, we also obtained broad $1/2^+$, $7/2^+$, $1/2^-$ and $3/2^-$ resonance states when

we neglected polarizability of the two-cluster subsystems. Allowing for cluster polarization gives us three wide resonances: $7/2_4^+$, $1/2_4^-$ and $3/2_1^-$.

The Faddeev equation methodology were applied in Ref. [40] to study bound and resonance states in ${}^9\Lambda\text{Be}$ within a macroscopic three-body model. Several effective $\alpha\Lambda$ interactions and a separable $\alpha\alpha$ interaction were involved to calculate the spectrum. The selected $\alpha\Lambda$ and $\alpha\alpha$ interactions lead to the overbound ground state of ${}^9\Lambda\text{Be}$ in Ref. [40]. As the spin-orbit interaction is neglected in [40], the $3/2^+$ and $5/2^+$ have the same energy. They are bound states, since they are located under the ${}^5\Lambda\text{He} + \alpha$ threshold. Three $3/2^-$ resonance states were found in Ref. [40], two of them are located below the three-cluster threshold and one above. The $3/2_3^-$ state from [40] lies between our $3/2_4^-$ and $3/2_5^-$ resonance states. The latter states have significantly larger widths than the width of the $3/2_3^-$ resonance state obtained in Ref. [40].

In Table VII we collected experimental data on the spectrum of the ${}^9\Lambda\text{Be}$ hypernucleus. The references are found in Ref. [39]. As we can see from Table VII, there is some consistency in experimental data only for the

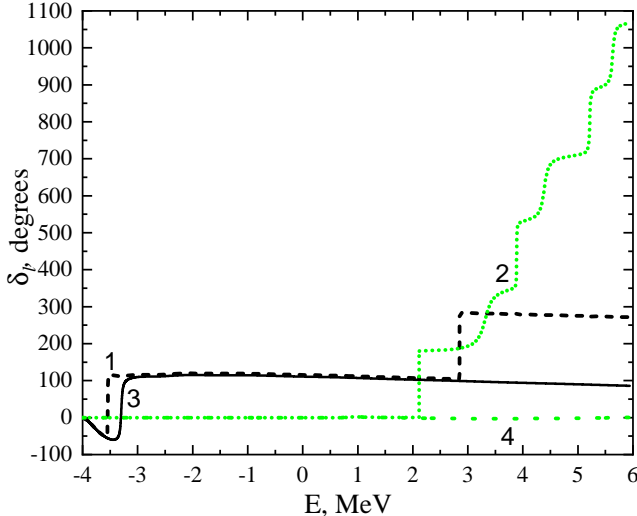


FIG. 3. Phase shifts of elastic many-channel scattering for $J^\pi = 3/2^+$ states of ${}^9\Lambda\text{Be}$ versus energy in the ${}^5\Lambda\text{He}(0_1^+) + {}^4\text{He}$ (1, 3) and ${}^8\text{Be}(0_1^+) + \Lambda$ (2, 4) channels. The data are obtained for soft (1, 2) and rigid (3, 4) two-cluster subsystems. Orbital momenta of the relative motion of clusters l_1 and l_2 equals 2.

TABLE VII. Spectrum of ${}^9\Lambda\text{Be}$ identified in different experiments

Source	[41, 42]		[16, 43]		[15, 44]	
	J^π	E , MeV	J^π	E , MeV	J^π	E , MeV
1/2 ⁺	-6.63	-5.90	1/2 ⁺	-6.63		
3/2 ⁺	-3.55	-2.97	5/2 ⁺	-3.606		
	6.40	-0.10	3/2 ⁺	-3.563		
	17.10	3.62		-0.83		
		8.98		2.89		
		11.23				
		13.64				
		17.50				

energies of the ground $1/2^+$ state and excited $3/2^+$, $5/2^+$ states. The energies of these three levels obtained within our model are in a good agreement with the experimental data from the first and last column.

C. Nature of the resonance states

As we can see above, our model generates a large number of resonance states in ${}^9\Lambda\text{Be}$. What is the nature of such resonance states? What factors are responsible for the appearance of these resonance states?

There are at least three possible reasons for the formation of resonance states and thus three types of resonances emerged in our many-channel model of ${}^9\Lambda\text{Be}$. First, the so-called shape resonance states can be created by a centrifugal or the Coulomb barriers, or by a combination of both barriers.

The centrifugal barrier is present in both ${}^5\Lambda\text{He} + \alpha$ and ${}^8\text{Be} + \Lambda$ channels, if the total orbital momentum and parity allow rotational states with nonzero orbital momentum of relative motion of the interacting clusters. The Coulomb barrier is present in the ${}^5\Lambda\text{He} + \alpha$ channel only. Effects of the Coulomb forces on parameters of the resonance states are demonstrated in Table V with $J^\pi = 3/2^+$ states. This example shows us that the Coulomb interaction is not responsible for creating such a rich variety of resonance states. As we have seen, it changes parameters of a resonance state and transforms a weakly bound state into a resonance state.

Second, some part of the obtained resonance states may be considered as the Pauli resonance states. Appearance of a large number of resonance states in cluster systems has been discovered many years ago (see, for example, Refs. [45–52]). In Refs. [53, 54] it has been shown with a simple two-cluster model systems how the Pauli resonances appear in the resonating group method calculations when different oscillator lengths are used for the interacting clusters. It is worthwhile noticing that with distinct values of oscillator lengths for different clusters one achieves more adequate description of a compound system. The Pauli resonance states may appear also in the case when the same oscillator lengths are used but more advanced internal cluster functions are adopted. Using different oscillator lengths implies invoking monopole excitations of each cluster. Such excitations in light nuclei have the energy around 20 MeV. And, consequently, the Pauli resonances appear in a high-energy range. Meanwhile, employment of more advanced wave functions of interacting clusters by considering them as a binary structure may result in a set of low-energy internal states which generate the Pauli resonances at a low energy. That is the case for the present investigation.

The Pauli resonances is caused by the almost Pauli forbidden states, which can be present in the wave function instead of the Pauli forbidden states both in the case of different oscillator lengths and advanced intrinsic cluster wave function. Recall that the forbidden states are the eigenfunctions of the norm kernel with zero eigenvalues, while the almost Pauli forbidden states correspond to nonzero but very small eigenvalues. In Ref. [55] it was claimed that the Pauli resonances disappear if the almost forbidden states are removed from the wave function. It was demonstrated for the ${}^{16}\text{O} + \alpha$ scattering that by omitting the eigenstates with eigenvalues less than 1.0×10^{-2} one removes the Pauli resonances. We apply this algorithm to calculate the $3/2^+$ phase shifts and parameters of the resonance states. In this case we have got only one almost forbidden state with the eigenvalue 6.4×10^{-8} . Other eigenvalues are spread in the region between 0.2 and 1.8. Elimination of the almost forbidden state did not result in changing phase shifts and parameters of the $3/2^+$ resonances. The same results were obtained for the $1/2^+$ and $1/2^-$ states. This let us conclude that the obtained resonances are not the Pauli resonances. We

suggest that the Pauli resonance states arise at a higher energy.

Third, Feshbach resonances appear in many-channel systems, provided that the channels have different threshold energies. The Feshbach resonance state originates from a bound states in one of the channels with a higher energy of the decay threshold. Having coupled with other channel(s) with lower threshold energy, the bound state may then decay through the open channel(s). If the coupling between channels is weak, the bound state turns into a resonance state. If the coupling is strong, a bound state can be dissolved by continuum. We have the necessary conditions for creation of the Feshbach resonance states, since the binary channels involved in the calculations have different threshold energies (see Table III). In the region $1 \text{ MeV} < E < 6 \text{ MeV}$, where we discovered the majority of the resonance states, there are four closed channels which can generate bound states.

However, to prove that our resonance states are the Feshbach resonances, we need to compare spectrum of the resonance states with the spectrum of bound states in closed binary channels treated separately. To obtain spectrum of the bound states, we selected from a huge matrix of the Hamiltonian those blocks which describe each channel and omitted the blocks which couple them. Thus problem of the N_{ch} coupled channels are reduced to the problem of N_{ch} independent channels and each channel is treated separately. As we pointed above, there is a weak coupling between different channels of ${}^9_{\Lambda}\text{Be}$. Thus we expect a correspondence between energies of the bound and resonance states.

Comparison is made in Fig. 4 where we display the energy of the $3/2^+$ resonance states created by the eight coupled channels (the middle spectrum) with the energy of bound states in the channel ${}^5_{\Lambda}\text{He}(0_3^+) + \alpha$ (the left spectrum) and channel ${}^8\text{Be}(0_3^+) + \Lambda$ (the right spectrum). We display only those bound states in all closed channels which lie in the energy range of our interest. Spectrum of bound states in each channel is obtained with 200 oscillator functions. By the dashed lines we indicated two- and three-body thresholds.

One can see in Fig. 4 that the energies of the resonance states obtained in the coupled-channel approximation are very close to the energies of the bound states calculated within a single-channel approximation. The ${}^5_{\Lambda}\text{He}(0_3^+) + \alpha$ closed channel generates three resonance states, while the ${}^8\text{Be}(0_3^+) + \Lambda$ closed channel creates four resonance states. Thus, the numerous resonance states emerged from our calculations are mainly the Feshbach resonance states. They complement the shape resonance states created by the centrifugal and Coulomb barriers which appear at the low-energy region.

Summarizing, we can conclude that the location of narrow resonances of the ${}^9_{\Lambda}\text{Be}$ hypernucleus in the energy region above ${}^8\text{Be}(0_1^+) + \Lambda$ threshold depends on the pseudo-bound states of the ${}^8\text{Be}$ and ${}^5_{\Lambda}\text{He}$ two-cluster subsystems, which have been taken into account. We can assume that the experimentally observed levels of the two-body

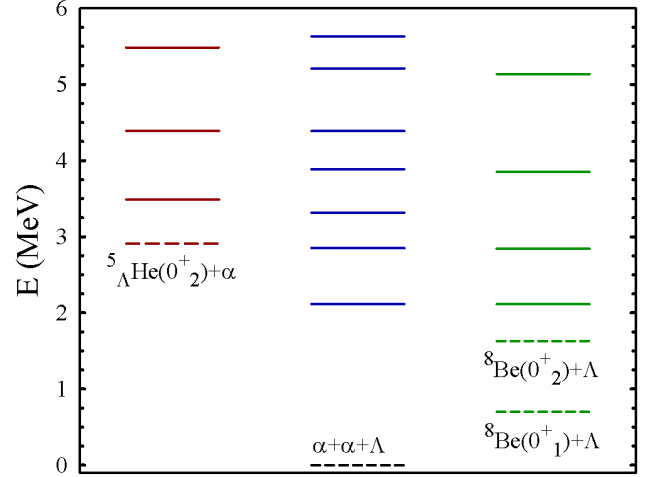


FIG. 4. Spectrum of the $3/2^+$ resonance states in ${}^9_{\Lambda}\text{Be}$ obtained in the coupled-channel approximation compared with the bound states created by closed binary channels treated separately

subsystems of the considered hypernucleus should be primarily accounted for. For the ${}^9_{\Lambda}\text{Be}$ hypernucleus these are 0^+ ground state and 2^+ , 4^+ resonance states of the ${}^8\text{Be}$ nucleus, as well as the 0^+ ground state of the ${}^5_{\Lambda}\text{He}$ hypernucleus. In the present paper, we properly accounted for the ground states of both two-body subsystems in the ${}^9_{\Lambda}\text{Be}$ hypernucleus. In addition, we allowed for both subsystems to be polarized without changing their angular momenta. There are strong grounds to believe that the location of the resonances of the ${}^9_{\Lambda}\text{Be}$ located below ${}^8\text{Be}(0_1^+) + \Lambda$ threshold remains unaffected by considering 2^+ and 4^+ pseudo-bound states of the ${}^8\text{Be}$ subsystem instead of already taken into account 0_2^+ , 0_3^+ and 0_4^+ states. However, it can change the energies of the ${}^9_{\Lambda}\text{Be}$ resonance states lying at the energy range $E > 2 \text{ MeV}$ above the three-cluster threshold.

IV. CONCLUSIONS

We have applied a microscopic three-cluster model to studying the structure of the ${}^9_{\Lambda}\text{Be}$ hypernucleus. The model treats correctly the Pauli principle and accounts for polarization of two-cluster subsystems of the hypernucleus when the third cluster is close by reducing a three-cluster problem to a coupled many-channel two-cluster problem. A Gaussian basis was used for the description of the two-cluster subsystems, while a harmonic oscillator basis was invoked for the relative motion of the two-cluster subsystem and the remaining cluster.

The hypernucleus ${}^9_{\Lambda}\text{Be}$ was considered as a three-cluster system comprising of two alpha particles and a Λ -hyperon. Within the present model the three-cluster

configuration was projected on two binary configurations ${}^5_{\Lambda}\text{He}+\alpha$ and ${}^8\text{Be}+\Lambda$, provided that ${}^5_{\Lambda}\text{He}$ and ${}^8\text{Be}$ were described as two-cluster systems. A finite number of Gaussian functions were used to describe $\alpha - \Lambda$ and $\alpha - \alpha$ binary subsystems. This resulted in a discretization of the continuous spectrum of ${}^5_{\Lambda}\text{He}$ and ${}^8\text{Be}$. The set of pseudo-bound states in ${}^5_{\Lambda}\text{He}$ and ${}^8\text{Be}$ allowed us to take into account polarizability of these systems.

The spectrum of bound and resonance states in the ${}^9_{\Lambda}\text{Be}$ hypernucleus was studied in detail. It was shown that the cluster polarizability plays a significant role in formation of bound and resonance states of this hypernucleus. Moreover, polarization of the two-cluster subsystems on interaction with the third cluster is responsible for creation of a large number of resonance states, a large part of them are very narrow with the total width less than 100 keV. We have shown that the majority of the narrow resonances in the energy range $1 \text{ MeV} < E < 6 \text{ MeV}$

are the Feshbach resonances generated due to a weak coupling of different binary channels in ${}^9_{\Lambda}\text{Be}$.

There is a fairly good agreement between our results and available experimental data. However, in our calculations the first $3/2^+$ excited state of the ${}^9_{\Lambda}\text{Be}$ is a resonance state, since it is located above the lowest ${}^5_{\Lambda}\text{He}+\alpha$ decay threshold of the ${}^9_{\Lambda}\text{Be}$. This can be ascribed to the selected nucleon-nucleon and nucleon-hyperon potentials which slightly overbind the ${}^5_{\Lambda}\text{He}$ subsystem. At the same time, the order of lowest $5/2^+$ and $3/2^+$ levels corresponds to the experimental data.

V. ACKNOWLEDGMENT

This work was supported in part by the Program of Fundamental Research of the Physics and Astronomy Department of the National Academy of Sciences of Ukraine (Project No. 0117U000239).

[1] V. S. Vasilevsky, F. Arickx, J. Broeckhove, and T. P. Kovalenko, Nucl. Phys. A **824**, 37 (2009), 0807.0136.

[2] Y. A. Lashko, G. F. Filippov, and V. S. Vasilevsky, Nucl. Phys. A **958**, 78 (2017).

[3] E. Hiyama and T. Yamada, Prog. Part. Nucl. Phys. **63**, 339 (2009).

[4] E. Hiyama, Y. Kino, and M. Kamimura, Prog. Part. Nucl. Phys. **51**, 223 (2003).

[5] E. Hiyama and M. Kamimura, Frontiers of Physics **13**, 132106 (2018), 1809.02619.

[6] Y. Kanada-En'yo, Phys. Rev. C **97**, 034324 (2018), 1801.01259.

[7] Y. Kanada-En'yo, Phys. Rev. C **97**, 024330 (2018), 1709.03375.

[8] R. Wirth, D. Gazda, P. Navrátil, and R. Roth, Phys. Rev. C **97**, 064315 (2018), 1712.05694.

[9] L. L. Margolin, in *European Physical Journal Web of Conferences* (2014), vol. 66, p. Di.

[10] E. Hiyama, Y. Yamamoto, T. Motoba, and M. Kamimura, Phys. Rev. C **80**, 054321 (2009), 0911.4013.

[11] O. Portilho, J. Phys. G Nucl. Phys. **25**, 961 (1999).

[12] E. Hiyama, M. Kamimura, T. Motoba, T. Yamada, and Y. Yamamoto, Phys. Rev. Lett. **85**, 270 (2000).

[13] T. Yamada, K. Ikeda, H. Band, and T. Motoba, Phys. Rev. C **38**, 854 (1988).

[14] Y. Funaki, T. Yamada, E. Hiyama, B. Zhou, and K. Ikeda, Prog. Theor. Exp. Phys. **2014**, 113D01 (2014), 1405.6067.

[15] H. Akikawa, S. Ajimura, R. E. Chrien, P. M. Eugenio, G. B. Franklin, J. Franz, L. Gang, K. Imai, P. Khaustov, and M. May, Phys. Rev. Lett. **88**, 082501 (2002).

[16] O. Hashimoto and H. Tamura, Prog. Part. Nucl. Phys. **57**, 564 (2006).

[17] M. Isaka and M. Kimura, Phys. Rev. C **92**, 044326 (2015), 1506.07238.

[18] W.-Y. Li, J.-W. Cui, and X.-R. Zhou, Phys. Rev. C **97**, 034302 (2018).

[19] M. Isaka, M. Kimura, A. Dote, and A. Ohnishi, Phys. Rev. C **83**, 044323 (2011), 1104.3940.

[20] A. Feliciello and T. Nagae, Rep. Prog. Phys. **78**, 096301 (2015).

[21] P. Veselý, E. Hiyama, J. Hrtánková, and J. Mareš, Nucl. Phys. A **954**, 260 (2016), 1605.05646.

[22] M. Theeten, D. Baye, and P. Descouvemont, Nucl. Phys. A **753**, 233 (2005).

[23] Y. Fujiwara, K. Miyagawa, M. Kohno, Y. Suzuki, D. Baye, and J. M. Spareenberg, Phys. Rev. C **70**, 024002 (2004), nucl-th/0404071.

[24] Y. Fujiwara, M. Kohno, K. Miyagawa, and Y. Suzuki, Phys. Rev. C **70**, 047002 (2004), nucl-th/0407039.

[25] E. Hiyama, M. Kamimura, T. Motoba, T. Yamada, and Y. Yamamoto, Prog. Theor. Phys. **97**, 881 (1997).

[26] J. Lee, Q. Wu, Y. Funaki, H. Zong, and E. Hiyama, Few-Body Systems **60**, 30 (2019).

[27] T. Motoba, H. Bandō, K. Ikeda, and T. Yamada, Prog. Theor. Phys. Suppl. **81**, 42 (1985).

[28] H. Bando, K. Ikeda, and T. Motoba, Prog. Theor. Phys. **69**, 918 (1983).

[29] K. Ikeda, H. Bandō, and T. Motoba, Prog. Theor. Phys. Suppl. **81**, 147 (1985).

[30] I. N. Filikhin and S. L. Yakovlev, Physics of Atomic Nuclei **63**, 336 (2000).

[31] R. Wirth, D. Gazda, P. Navrátil, A. Calci, J. Langhammer, and R. Roth, Phys. Rev. Lett. **113**, 192502 (2014), 1403.3067.

[32] J. Haidenbauer and U.-G. Meißner, Phys. Rev. C **72**, 044005 (2005), nucl-th/0506019.

[33] R. F. Barrett, B. A. Robson, and W. Tobocman, Rev. Mod. Phys. **55**, 155 (1983).

[34] A. Hasegawa and S. Nagata, Prog. Theor. Phys. **45**, 1786 (1971).

[35] F. Tanabe, A. Tohsaki, and R. Tamagaki, Prog. Theor. Phys. **53**, 677 (1975).

[36] E. Hiyama, Y. Yamamoto, T. A. Rijken, and T. Motoba, Phys. Rev. C **74**, 054312 (2006), nucl-th/0610019.

- [37] B. F. Gibson and I. Hungerford, E. V., *Phys. Rep.* **257**, 349 (1995).
- [38] V. O. Kurmangaliyeva, N. Kalzhigitov, N. Takibayev, and V. S. Vasilevsky, arXiv e-prints arXiv:2006.04525 (2020), 2006.04525.
- [39] J. Lee, Q. Wu, Y. Funaki, H. Zong, and E. Hiyama, *Few-Body Syst.* **60**, 30 (2019).
- [40] S. Oryu, H. Kamada, H. Sekine, H. Yamashita, and M. Nakazawa, *Few-Body Syst.* **28**, 103 (2000).
- [41] M. May, S. Bart, S. Chen, R. E. Chrien, D. Maurizio, P. Pile, Y. Xu, R. Hackenburg, E. Hungerford, H. Piekarz, et al., *Phys. Rev. Lett.* **51**, 2085 (1983).
- [42] W. Brückner, B. Granz, D. Ingham, K. Kilian, U. Lynnen, J. Niewisch, B. Pietrzyk, B. Povh, H. G. Ritter, and H. Schröder, *Phys. Lett. B* **62**, 481 (1976).
- [43] S. Ajimura, K. Aoki, H. Bhang, T. Endo, Y. Fujii, O. Hashimoto, H. Hotchi, E. Hungerford, J. H. Kim, Y. D. Kim, et al., *Nucl. Phys. A* **639**, 93 (1998).
- [44] H. Tamura, S. Ajimura, H. Akikawa, D. E. Alburger, K. Aoki, A. Banu, R. E. Chrien, G. B. Franklin, J. Franz, and Y. Fujii, *Nucl. Phys. A* **754**, 58 (2005), nucl-ex/0411028.
- [45] D. R. Thompson and Y. C. Tang, *Phys. Rev.* **179**, 971 (1969).
- [46] D. R. Thompson and Y. C. Tang, *Phys. Rev. C* **8**, 1649 (1973).
- [47] D. Clement, E. W. Schmid, and A. G. Teufel, *Phys. Lett. B* **49**, 308 (1974).
- [48] D. J. Stubeda, Y. Fujiwara, and Y. C. Tang, *Phys. Rev. C* **26**, 2410 (1982).
- [49] H. Kanada, T. Kaneko, and Y. C. Tang, *Nucl. Phys. A* **380**, 87 (1982).
- [50] H. Walliser and T. Fliessbach, *Nucl. Phys. A* **394**, 387 (1983).
- [51] H. Walliser, T. Fliessbach, and Y. C. Tang, *Nucl. Phys. A* **437**, 367 (1985).
- [52] H. Kanada, T. Kaneko, and Y. C. Tang, *Phys. Rev. C* **38**, 2013 (1988).
- [53] T. Fliessbach and H. Walliser, *Nucl. Phys. A* **377**, 84 (1982).
- [54] H. Kanada, T. Kaneko, and S. Saito, *Prog. Theor. Phys.* **54**, 747 (1975).
- [55] M. Kruglanski and D. Baye, *Nucl. Phys. A* **548**, 39 (1992).